arXiv:1603.08977v1 [astro-ph.SR] 29 Mar 2016

Stochastic transients as a source of quasi-periodic processes in the solar atmosphere

Ding Yuan[1,2]
DYuan2@uclan.ac.uk

Jiangtao Su[2]

Fangran Jiao[3]

Robert W. Walsh[1]

ABSTRACT

Solar dynamics and turbulence occur at all heights of the solar atmosphere and could be described as stochastic processes. We propose that finite lifetime transients recurring at a certain place could trigger quasi-periodic processes in the associated structures. In this study, we developed a mathematical model for finite lifetime and randomly occurring transients, and found that quasi-periodic processes, with period longer than the time scale of the transients, are detectable intrinsically in form of trains. We simulate their propagation in an empirical solar atmospheric model with chromosphere, transition region and corona. We found that, due to the filtering effect of the chromospheric cavity, only the resonance period of the acoustic resonator is able to propagate to the upper atmosphere, such a scenario is applicable to slow magnetoacoustic waves in sunspots and active regions. If the thermal structure of the atmosphere is less wild and acoustic resonance does not take effect, the long period oscillations could propagate to the upper atmosphere. Such case would be more likely to occur at polar plumes.

Subject headings: Sun: atmosphere — Sun: corona — Sun: oscillations — magnetohydrodynamics (MHD) — waves

1. Introduction

A variety of solar transients and turbulence occurs at the layers close to the visible surface of the Sun: convections (Nordlund et al. 2009; Stein 2012), granulations (Rieutord & Rincon 2010), magnetic reconnections (heatings or flares, Hannah et al. 2011; Cargill et al. 2015), spicular activities (De Pontieu et al. 2007b), etc. These activities have finite lifetimes and repeat at the same location without nominal periodicities. However, the nature of intermittency in conjunction with finite lifetimes could well lead to a quasi–periodic process in the associated structures.

In this paper, we aim to propose the idea that stochastic, finite lifetime transients could generate quasi-periodic processes in upper atmosphere of the Sun. This is inspired by the recent discoveries of low–amplitude intermittent transverse oscillations of corona loops (Nisticò et al. 2013; Anfino-

[1]Jeremiah Horrocks Institute, University of Central Lancashire, Preston, PR1 2HE, United Kingdom

[2]Key Laboratory of Solar Activity, National Astronomical Observatories, Chinese Academy of Sciences, Beijing, 100012, China

[3]Shandong Provincial Key Laboratory of Optical Astronomy and Solar-Terrestrial Environment, Institute of Space Sciences, Shandong University, Weihai, 264209 Shandong, China

gentov et al. 2013, 2015), and the connectivity between spicular activities and quasi-periodic propagating disturbances in coronal holes (Jiao et al. 2015; Samanta et al. 2015). **The quasi-periodic fast wave trains may also be launched by intermittent impulsive pertubations to reconnection sites (Yuan et al. 2013; Pascoe et al. 2013; Nisticò et al. 2014; Yang et al. 2015)**. We demonstrate the feasibility of this idea by studying how stochastic spicules are connected with propagating disturbances observed in coronal holes and active regions. However, we believe this idea is applicable to other temporal and spatial scales in solar and astrophysics.

Spicules are rapidly evolving elongated transients observed off the solar limb (Beckers 1968; Sterling 2000); while mottles and dynamic fibrils, observed at quiet-Sun and active region plages, respectively, are suggested to be the on-disk counterparts of spicules (Hansteen et al. 2006; De Pontieu et al. 2007a; Rouppe van der Voort et al. 2009). Two classes of spicules are identified by De Pontieu et al. (2007b), although scepticism remains (Sterling et al. 2010; Zhang et al. 2012). Type I spicules are relatively slowly evolving features, and will eventually fall back due to gravity on a time scale of $3-7$ min (De Pontieu et al. 2007b); Type II spicules will fade off into the background within a lifetime of about 45 s (and a spread about $10-150$ s) (De Pontieu et al. 2007b).

Spicular activity or its on-disk counterpart are believed to be associated with the excessive blue-shifted spectral line emission (upward flows) observed at the footpoints of active regions (Del Zanna 2008; Doschek et al. 2008; Hara et al. 2008; Tian et al. 2011). Upon observing persistent upflows and correlated linewidth and intensity variations, McIntosh & De Pontieu (2009),De Pontieu & McIntosh (2010) and Tian et al. (2011) intepreted propagating disturbances observed at footpoints of active region loops as quasi-periodic upflows. However, periodic flows rarely occur in nature, unless they are modulated or waveguided by other thermal or magnetic structures. This idea will be demonstrated in this study. A rival theory is propagating slow mode magnetohydrodynamics (MHD) wave: the propagating disturbances have good periodicy (Nakariakov et al. 2000; King et al. 2003; De Moortel 2009) and a natural source of sunspot oscillations (Yuan et al. 2014b,a; Tian et al. 2014; Su et al. 2016a,c); the intensity (or density) and velocity disturbances oscillate in phase (Wang et al. 2009a,b); the phase speed is temperature-dependent and always smaller than local acoustic speed (Marsh et al. 2009; Kiddie et al. 2012; Uritsky et al. 2013); moreover, propagating slow wave could also produce blue-shifted line emission (Verwichte et al. 2010), albeit with half wave period.

Recent simulations suggest upflows will inevitably excite slow waves in active region loops and that a blend of both upflows and slow wave may contribute to the observational features in coronal loops (Ofman et al. 2012; Wang et al. 2013). Fang et al. (2015) demonstrates that impulsive heating at the footpoint of a coronal loop will trigger pressure imbalance and excite high-speed upflows. However, as long as the flow become detached with the source, it evolves as a slow wave pulse. Jiao et al. (2015) and Samanta et al. (2015) found compelling evidence that propagating disturbances at polar plumes have strong correlation with the spicular activities at chromospheric height. Similar dynamics (dynamics fibrils) are observed at active regions (Skogsrud et al. 2016).

In this paper, we propose the idea that quasi-periodicity processes are intrinsic part of stochastic finite lifetime transients, and simulate the propagation of stochastic spicules in the solar atmosphere. Section 2 describes the mathematical model of stochastic transients; Section 3 presents the numerical experiment to demonstrate the idea; Section 4 compares the synthetic data and Solar Dynamics Observatory (SDO)/Atmospheric Imaging Assembly (AIA) observations at active regions and polar plumes.

2. Model of stochastic transients

We model a set of sequential transients $g_i(t_i)$ with a peak strength at t_i. For simplicity, we assume each transient evolves in an Gaussian profile with an amplitude of v_i and a width of σ_i:

$$v(t) = \sum_{i=1}^{N} g_i(t_i) = \sum_{i=1}^{N} v_i \exp\left[\frac{-(t-t_i)^2}{2\sigma_i^2}\right], \quad (1)$$

$$t_i = iP_0 + \delta t_i, \quad (2)$$

$$\sigma_i = \sigma_0 + \delta\sigma_i. \quad (3)$$

The amplitude v_i is an random number that follows a uniform distribution $v_0\mathcal{U}(0,1)$. A transient is assumed to be launched every P_0 and shifted by a normally distributed random offset δt_i, where $\delta t_i/P_1$ has a normal distribution $\mathcal{N}(0,1)$. So the occurrence interval $t_{i+1}-t_i$ has an average value of P_0 and a standard deviation of $\sqrt{2}P_1$. The width σ_i of a transient, relating to its lifetime, has a nominal value of σ_0 and a random variation $\delta\sigma_i$; and $\delta\sigma_i/\sigma_1$ follows a normal distribution $\mathcal{N}(0,1)$. To reduce the number of free parameters, we fix $P_1 = P_0/2$, which allows a small probability that two consecutive transients overlap to some extent. We also set $\sigma_1 = \sigma_0/4$, so that σ_i is unlikely to be negative. Tests show that even σ_1 is set to zero or other reasonable values, the spectrum of the time series remains slightly altered. Similar tests were performed on P_1, we did not find significant changes to the spectrum. To see the feasibility of this idea, we introduce typical time scales of the dynamics commonly observed in the lower atmosphere of the Sun.

Type-I spicules have dynamic time scales at $3-7$ min and lifetimes at $2-3$ min (De Pontieu et al. 2007b); Mottles and fibrils are found to have similar time scales (Hansteen et al. 2006; De Pontieu et al. 2007a; Rouppe van der Voort et al. 2009). So we used $P_0 = 300$ s, and $\sigma_0 = 100$ s to simulate the time series associated by spicular dynamics, see Figure 1(a). **The time series is analysed by wavelet transform to show the dynamic spectrum. We applied the Morlet mother function, which is optimised for revealing the oscillatory signals (Torrence & Compo 1998). In the wavelet spectrum, we only plot the spectral component above the 90% confidence level. This standard is followed in other wavelet spectra throughout this paper.** Spectral peaks aggregate at about $0.5-1.5$ mHz (10–30 min, Figure 1(b)). Power spectrum of quasi-periodic propagating disturbances observed at coronal holes exhibit periodicities at exactly the same frequency range (McIntosh et al. 2010; Krishna Prasad et al. 2011a, 2012; Banerjee et al. 2011).

Type-II spicules recur more frequently (about every 60 s) and shorter-lived (about 40 s). Shorter time scales are found in nanoflares and high-frequency heatings (Porter et al. 1984; Parker 1988; Klimchuk 2015). We use $P_0 = 80$ s, and $\sigma_0 = 30$ s to model the dynamics of these time scales; prominent periodicities are found at **2-8 min and 50-70 min bands** (Figure 2). Short period propagating disturbances in coronal holes and active regions (e.g., De Moortel 2009; Banerjee et al. 2011; Yuan & Nakariakov 2012) and sunspot oscillations (e.g., Yuan et al. 2014a,b; Tian et al. 2014; Su et al. 2016b) situate in **2-8 min** period range.

3. Numerical experiments

In order to explore how stochastic transients affect the upper atmosphere, we set up a set of numerical experiments, and investigate how the power spectrum is altered observationally throughout its propagation in a stratified atmosphere. We do not attempt to model realistic transients at photospheric temperature and density, but only demonstrate if this sort of perturbations was triggered at the lower atmosphere, what would be the response that could be observed.

3.1. Empirical atmosphere model

Figure 3 plots the one-dimensional atmosphere model used in this study. Below $z < 2.22$ Mm, we implemented the Maltby et al. (1986) mid-age sunspot umbra model; close to the bottom boundary ($z < 1.2$ Mm), we set a constant temperature (6471 K). Above $z = 2.22$ Mm, we adapted the Avrett & Loeser (2008) C7 model; and near the upper boundary ($z \in [36\,\mathrm{Mm}, 40\,\mathrm{Mm}]$), we put a constant temperature at 1.3 MK. This kind of temperature model has been used in a number of previous studies, e.g., Heggland et al. (2007); Botha et al. (2011); Snow et al. (2015).

In hydrostatic equilibrium, the pressure is obtained by integrating the gravity force ρg,

$$p(z) = p(0)\exp\left[\int_0^z -\rho g \mathrm{d}z\right] \tag{4}$$

$$p(z) = \frac{\rho(z) k_\mathrm{B} T(z)}{0.5 m_\mathrm{p}}, \tag{5}$$

where p, ρ and T are the plasma pressure, density and temperature, respectively, $g = 275.43\,\mathrm{m\cdot s^{-2}}$ is the gravitational constant, k_B is the Boltzmann constant, m_p is the mass of proton. We choose a base density of $\rho(0) = 6.6\cdot10^{-8}\,\mathrm{kg\cdot m^{-3}}$ at $z = 0$ Mm, so at coronal height the density is

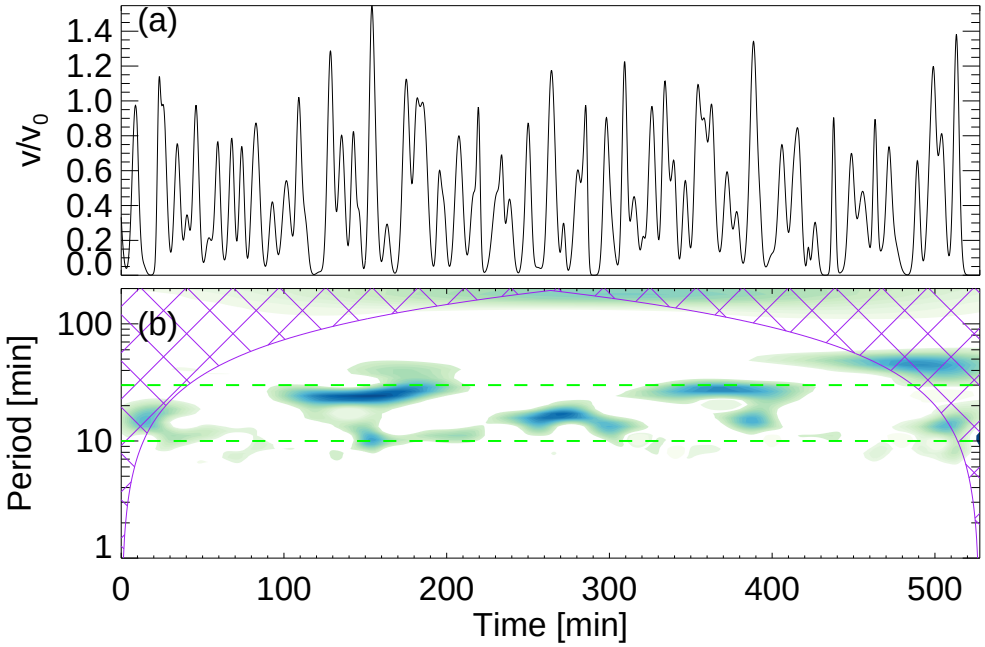

Fig. 1.— (a) Time series of stochastic finite lifetime transient model. (b) Wavelet spectrum illustrates quasi-periodic oscillations at 10-30 min range, enclosed within the green dashed lines. The Cone-of-Influence is cross-hatched, within which spectrum should be considered as unreliable. We used $P_0 = 300\,\mathrm{s}$ and $\sigma_0 = 100\,\mathrm{s}$.

of the order of $10^{-13}\,\mathrm{kg\cdot m^{-3}}$, see Figure 3. In one-dimensional MHD simulation, the magnetic field decouples from hydrodynamic equilibrium; we used $B = 10\,\mathrm{G}$, in line with the z-axis, in our simulations.

The plasma parameters were normalized by choosing a set of three constant: the length $L_0 = 1.0\,\mathrm{Mm}$, the density $\rho_0 = 8.0\cdot10^{-10}\,\mathrm{kg\cdot m^{-3}}$, and the magnetic field strength $B_0 = 10\,\mathrm{G}$. Then the normalization factor for the velocity is $V_0 = 31.6\,\mathrm{km\cdot s}$, the time $t_0 = 31.7\,\mathrm{s}$, the gravitational constant $g_0 = 997\,\mathrm{m\cdot s^{-2}}$, the temperature $T_0 = 0.06\,\mathrm{MK}$. So the variables become dimensionless by using $z = \hat{z}L_0$, $\rho = \hat{\rho}\rho_0$, $B = \hat{B}B_0$, $t = \hat{t}t_0$, $v = \hat{v}V_0$, $g = \hat{g}g_0$, $p = \hat{p}p_0$, $T = \hat{T}T_0$ etc, where symbols with a hat are dimensionless variables.

3.2. Magnetohydrodynamic simulation

We used the AMRVAC package (Keppens et al. 2012; Porth et al. 2014) to solve the ideal MHD equations with finite-volume method:

$$\frac{\partial\rho}{\partial t} + \nabla\cdot(\rho\mathbf{v}) = 0, \tag{6}$$

$$\frac{\partial\rho\mathbf{v}}{\partial t} + \nabla\cdot\left[\rho\mathbf{v}\mathbf{v} + \mathbf{I}p_{\rm tot} - \frac{\mathbf{B}\mathbf{B}}{\mu_0}\right] = \rho\mathbf{g}, \tag{7}$$

$$\frac{\partial\epsilon}{\partial t} + \nabla\cdot\left[\mathbf{v}(\epsilon + p_{\rm tot}) - \frac{(\mathbf{v}\cdot\mathbf{B})\mathbf{B}}{\mu_0}\right] = \rho\mathbf{g}\cdot\mathbf{v}, \tag{8}$$

$$\frac{\partial\mathbf{B}}{\partial t} + \nabla\cdot(\mathbf{v}\mathbf{B} - \mathbf{B}\mathbf{v}) = 0, \tag{9}$$

$$\epsilon = \frac{1}{2}\rho v^2 + \frac{p}{\gamma-1} + \frac{B^2}{2\mu_0}, \tag{10}$$

where $\mathbf{v}$ is the fluid velocity, $\mathbf{B}$ the magnetic field vector, $\mathbf{g} = -g\mathbf{z}$ the solar gravity vector, **I unit tensor,** ϵ **the total energy density,** $p_{\rm tot} = p + B^2/2\mu_0$ **total pressure,** γ the adiabatic index, and μ_0 the magnetic permeability of free space.

The AMRVAC code was configured to solve Equations 6-10 in Cartesian coordinates $[x, y, z]$. The physical quantities were assumed to be invariant along the x- and y-axes (i.e., $\partial/\partial x = \partial/\partial y = 0$). We exploited the HLL approximate Riemann

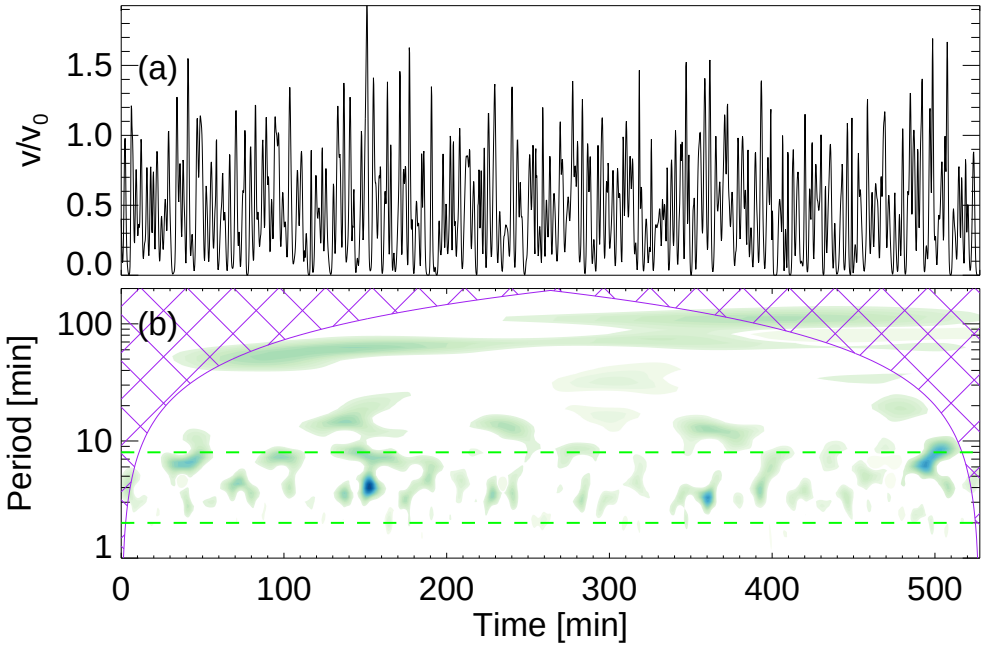

Fig. 2.— Same as Figure 1, but $P_0 = 80\,\mathrm{s}$ and $\sigma_0 = 30\,\mathrm{s}$. Green dashed lines label the prominent quasi-periodic oscillations at 2-8 min range. The Cone-of-Influence is cross-hatched, within which spectrum should be considered as unreliable.

solver (Harten et al. 1983) and implemented the KOREN flux limiter (Koren 1993). A three-step Runge-Kutta method was used in time discretization. This configuration has been used in Yuan et al. (2015a) to study propagating fast waves in randomly structured plasmas.

A solution domain was set at $z \in [0\,\mathrm{Mm}, 40\,\mathrm{Mm}]$. At the top boundary, we extrapolated values for the density and pressure; mirroring boundary condition was used for the velocity to minimize reflections. At the bottom boundary we fixed the values of plasma density and pressure, extrapolated from the empirical atmosphere model; the velocity was set up according to the driver model, see Section 2. We used 4000 fixed grid cells without adaptive mesh refinement, so cell size was $\mathrm{d}z = 10\,\mathrm{km}$. We relaxed the system till $t/t_0 = 50$, the maximum velocity caused by numerical noise is 0.003 (i.e., $0.1\,\mathrm{km \cdot s^{-1}}$). So we could consider the system already in hydrostatic equilibrium, and drivers could be applied at $t/t_0 = 0$.

3.3. Single pulse test

Our model contains an acoustic resonator for slow magnetoacoustic waves: the slow waves get reflected at the sharp density gradient when propagating downwards, and encounter cut-off effect at the upper atmosphere (Roberts 2006; Afanasyev & Nakariakov 2015). Theory of the acoustic resonator model could be found in Zhugzhda (2008); Zhugzhda et al. (1983), and simulations in Botha et al. (2011) and Snow et al. (2015).

A single Gaussian pulse with $\sigma_i = 100\,\mathrm{s}$ was launched at the bottom boundary. The pulse reached the height at about 2 Mm after about 2 minutes, the average phase speed was about $15\,\mathrm{km \cdot s^{-1}}$ (Figure 4(a)). Above 2 Mm, the density drops dramatically, and shock wave started to form, which is the suggested formation mechanism for chromospheric jets and spicules (Heggland et al. 2007; De Pontieu et al. 2007b). The pulse energy did not completely penetrate through the transition region and went off; a significant portion of energy was trapped within the acoustic resonator, bouncing back and forth, see Fig-

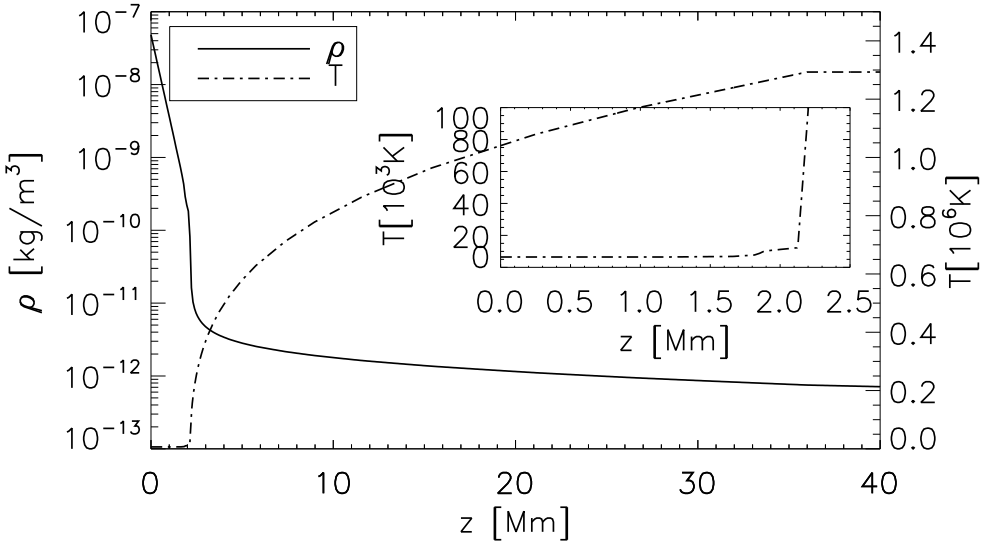

Fig. 3.— Empirical atmosphere model used in this study, the zoomed-in panel plots temperature profile at $z < 2.5$ Mm.

ure 4(c). The wavelet spectrum of the density perturbation within the resonator $z = 1.8$ Mm ($T \sim 7000$ K, Figure 4(e)) reveals that the pulse initially carried a broadband of signals, and quick involved into a monochromatic oscillation with a period of about 5 min. The phase difference between the density and velocity perturbation was initially zero and rapidly split into $\pi/4$ (Figure 4(c)), which means a standing slow wave was formed within the resonator (Wang 2011; Yuan et al. 2015b). At the coronal height, we extracted time series at $z = 10$ Mm ($T \sim 0.8$ MK). The signal was quasi-periodic (Figure 4(f)); and density and velocity oscillated almost in phase (Figure 4(d)), meaning propagating slow wave was observed at corona heights (also see Wang et al. 2009a,b; Yuan & Nakariakov 2012; Fang et al. 2015). The average propagating speed was about $100\,\mathrm{km}\cdot\mathrm{s}^{-1}$. Owing to the lack of persistent energy supply, the slow wave decayed off within a few cycles.

Our result is consistent with the theory of dispersive evolution of impulsive disturbance in stratified atmosphere (Chae & Goode 2015). However, we get longer period (or lower resonance frequency) than Botha et al. (2011), this is because we used a less wild temperature profile, thus relative smaller density gradient. It also implies that the resonance frequency is a good probe to the resonator's thermal structure, which may evolve with the age of a sunspot or other solar structures (Zhugzhda et al. 1983; Zhugzhda 2008). We shall note that in the simulations of Heggland et al. (2007), periodic drivers are applied; the effect of the resonator is barely seen. This may be owe to the fact that they aim at simulating shock waves with large amplitudes and thus render the trapped energy less prominent. However, irregularities of the shock fronts could be seen in Figure 11 of Heggland et al. (2007), which may be the signature of the trapped energy.

3.4. Perturbation by stochastic transients

After the single pulse experiment, we applied the stochastic transients model (Equation 1), times series and parameters are illustrated in Figure 1. Figure 5 presents time distance plots of density and velocity, and the time series and relevant wavelet analysis. Shock waves are formed at a height where density drops dramatically (Figure 5(a)), the amplitude could be as large as 60% of the background density (Figure 5(c)). At $z = 1.8$ Mm, the phase between density and velocity perturbations have mixed feature, while at $z = 10$ Mm, it is almost zero, indicating that propagating slow waves are found at the coronal height. The wavelet spectrum reveals that at

$z = 1.8$, long period oscillations ($10 - 30$ min) and the resonance period ($\sim$ 5 min) co-exist within the acoustic resonator (Figure 5(e)); while only the resonance period is allowed to leak from chromosphere (Figure 5(f)). This is consistent with Snow et al. (2015), who demonstrated that even long period oscillations are implemented in the driver, their power would be 2-3 orders of magnitude smaller than the resonance period. Long period oscillations are indeed observed at active regions and other coronal structures (Wang et al. 2009b; Marsh et al. 2009; Yuan et al. 2011); this effect is ascribed to modification to the cut-off period of slow wave by inclined magnetic field, see Bel & Leroy (1977); McIntosh & Jefferies (2006); Jess et al. (2013); Yuan et al. (2014b); Afanasyev & Nakariakov (2015).

We also notice that the resonance within the acoustic cavity and the leakage to the corona are not persistent, but forms a series of wave trains. This is a novel feature that no other study could be able to simulate, and it is consistent with the fact that propagating disturbances at active region loops are detected in forms of wave trains (De Moortel 2009; De Moortel & Nakariakov 2012). Moreover, the mixture of both long period and short period oscillations in the acoustic resonator is remarkably similar to the sunspot oscillations observed at chromospheric height using the Nobeyama RadioHeliograph (Chorley et al. 2010, 2011).

Long period oscillations are also detected at coronal plumes (Ofman et al. 1999; Gupta et al. 2010; Krishna Prasad et al. 2011b; Jiao et al. 2015), At low corona, the magnetic field pressure dominates over gas pressure, a plume could be simply assumed to be isothermal (Del Zanna et al. 1998). In this study, we did not use an isothermal model, but simply apply the driver at $z = 2.3$ Mm, and demonstrate that altering the thermal structure of the solar atmosphere could also lead to the leakage of long period oscillations.

Figure 6 presents the result if we apply the driver at $z = 2.3$ Mm ($T = 0.1$ MK); this scenario skip the chromospheric cavity. In contrast to being launched deeper, the density and velocity perturbations do not form shock waves, but stay at small amplitude level (Figure 6(c) and (d)). The long period wave trains manage to propagate into coronal heights.

4. Observations in the solar atmosphere

4.1. Oscillations in sunspot and active region loops

In the solar atmosphere, thermal structure of a sunspot and the associated active region (AR) resembles the used empirical atmospheric model (see Section 3.1). Therefore, we selected a 5-hours AIA observation on AR 11504 (Figure 7). The start time is 16:00:00 UT 14 June 2012. We used the AIA 304 Å and 171 Å channels, which have nominal response temperatures at 85,000 K (He II) and 850,000 K (Fe IX), respectively (Boerner et al. 2012). This AR has already been studied intensively in Su et al. (2013). A coronal loop anchoring at the trailing spot of AR 11504 was tracked (Figure 7). We extracted time series of the emission intensity in AIA 304 Å and 171 Å, removed the trend of a 30 min running average, and normalized the amplitude to ± 0.5. Figure 8 plots the time series and the relevant wavelet analysis. **Although we cannot guarantee that two time series were taken at two different heights of the same loop, but the oscillations at diffuse coronal structures have a correlation area of about 10 Mm long and a few Mm wide (De Moortel et al. 2002b), within which the wavelet spectrum is barely altered. So the ambiguity owe to the projection effect will not affect our conclusions.**

We could see that in both AIA 304 Å and 171 Å channels, one could detect prominent oscillations at three minute in form of wave trains (Figure 8), which has been reported in a number of studies (e.g., De Moortel et al. 2002a; King et al. 2003; Yuan et al. 2014b). In the meanwhile, we also detect significant long period oscillations at $10 - 30$ min at both heights. The leakage of long period oscillations was studied previous, e.g.,Yuan et al. (2011), Marsh et al. (2009), Wang et al. (2009b). The mechanism for the leakage is not fully understood: the inclined magnetic field could lower cut-off frequency (De Pontieu et al. 2005; McIntosh & Jefferies 2006; Yuan et al. 2014b), evanescent slow waves with long penetration depths re-gain propagating wave feature at coronal heights (Fleck & Schmitz 1991; Yuan et al. 2011), or long period oscillations are somehow generated at coronal height.

To compare with the observational data, we

synthesized the AIA 304 Å and 171 Å emission intensities (details of forward modelling is available at Yuan et al. 2015b; Fang et al. 2015), by using the CHIANTI atomic emission database (Dere et al. 1997; Landi et al. 2013). Figure 9 presents the time-distance plots, the time series extracted at $z = 6$ Mm (304 Å) and 10 Mm (171 Å) and the associated wavelet analysis. The time series for the synthetic AIA 304 Å and 171 Å emission intensities exhibit only oscillations at the resonance period ($\sim$ 5 min); while long period oscillations are occasionally detected at low confidence level. In our simulation, the magnetic field line is vertical; the magnetoacoustic cut-off frequency is not modified at all. In an active region, magnetic field are bent to connect another polarity, so significant long period oscillations are more likely to be detected (Yuan et al. 2011, 2014b).

4.2. Propagating disturbances in polar plumes

To investigate the oscillations in polar plumes, we select a set of 4-hours AIA observations on a coronal hole, starting from 21:50 UT 5 August 2010. A few polar plumes are identifiable at low corona in the AIA 171 Å channel, and their bases could be well traced in the AIA 304 Å channel (Figure 10). The plume structure enclosed in rectangle are chosen for further analysis. We extracted the average emission intensity within the small boxes in the 304 Å and 171 Å FOVs, respectively. We used the original light curves of 304 Å bandpass, while for the 171 Å bandpass, we removed a trend of the 30 min moving average and smoothed the time series. The amplitudes are normalized to $[\pm 0.5]$. Long period oscillations at $10 - 30$ min are apparent in the light curve and wavelet spectrum of 304 Å and 171 Å (Figure 11).

Similar procedures are implemented to the simulation with driver launched at $z = 2.3$. Figure 12 illustrates the forward modelling result to compare with oscillations in polar plumes. **Indeed, the long period oscillations propagate to coronal height, and are detectable in the UV/EUV bandpasses.**

In the simulation, we only use the time scale of spicular activities that are found to be highly correlated with quasi-periodic propagating disturbances in polar plumes (Jiao et al. 2015; Samanta et al. 2015). However, as Krishna Prasad et al. (2012) shows multiple periods co-exist in the propagating disturbances, therefore other time scale are needed to fully address this issue.

5. Conclusions

In this study, we propose that stochastic, finite-life time transients could generate quasi-periodic processes in the solar atmosphere; and we suggest an mathematical model of stochastic transients in form of Gaussian profiles. Then we use the typical time scales of spicular activities and simulate the propagation of stochastic transients in an empirical atmosphere model. The existence of an chromospheric resonator filters out the long period oscillations, only the resonance period is able to propagate to the upper atmosphere. Observations with SDO/AIA 304 Å and 171 Å bandpasses, which are sensitive to the chromospheric and coronal heights, produce consistent results. We also investigate the case that the thermal structure are changed into a smoother form and the acoustic resonator does not exist. Such a scenario is applicable to polar plumes. Indeed, both simulations and observations clearly measures significant long period oscillations.

Our model is applicable to many field in geophysics, solar, stellar and astrophysics. The time scale could scaled to any range of interest, we only provide a possible application.

The research was supported by the Open Research Program KLSA201504 of Key Laboratory of Solar Activity of National Astronomical Observatories of China (D.Y.).

REFERENCES

Afanasyev, A. N., & Nakariakov, V. M. 2015, A&A, 582, A57

Anfinogentov, S., Nisticò, G., & Nakariakov, V. M. 2013, A&A, 560, A107

Anfinogentov, S. A., Nakariakov, V. M., & Nisticò, G. 2015, A&A, 583, A136

Avrett, E. H., & Loeser, R. 2008, ApJS, 175, 229

Banerjee, D., Gupta, G. R., & Teriaca, L. 2011, Space Sci. Rev., 158, 267

Beckers, J. M. 1968, Sol. Phys., 3, 367

Bel, N., & Leroy, B. 1977, A&A, 55, 239

Boerner, P., Edwards, C., Lemen, J., et al. 2012, Sol. Phys., 275, 41

Botha, G. J. J., Arber, T. D., Nakariakov, V. M., & Zhugzhda, Y. D. 2011, ApJ, 728, 84

Cargill, P. J., Warren, H. P., & Bradshaw, S. J. 2015, Philosophical Transactions of the Royal Society of London Series A, 373, 20140260

Chae, J., & Goode, P. R. 2015, ApJ, 808, 118

Chorley, N., Foullon, C., Hnat, B., Nakariakov, V. M., & Shibasaki, K. 2011, A&A, 529, A123

Chorley, N., Hnat, B., Nakariakov, V. M., Inglis, A. R., & Bakunina, I. A. 2010, A&A, 513, A27

De Moortel, I. 2009, Space Sci. Rev., 149, 65

De Moortel, I., Ireland, J., Hood, A. W., & Walsh, R. W. 2002a, A&A, 387, L13

De Moortel, I., Ireland, J., Walsh, R. W., & Hood, A. W. 2002b, Sol. Phys., 209, 61

De Moortel, I., & Nakariakov, V. M. 2012, Philosophical Transactions of the Royal Society of London Series A, 370, 3193

De Pontieu, B., Erdélyi, R., & De Moortel, I. 2005, ApJ, 624, L61

De Pontieu, B., Hansteen, V. H., Rouppe van der Voort, L., van Noort, M., & Carlsson, M. 2007a, ApJ, 655, 624

De Pontieu, B., & McIntosh, S. W. 2010, ApJ, 722, 1013

De Pontieu, B., McIntosh, S., Hansteen, V. H., et al. 2007b, PASJ, 59, S655

Del Zanna, G. 2008, A&A, 481, L49

Del Zanna, L., von Steiger, R., & Velli, M. 1998, Space Sci. Rev., 85, 349

Dere, K. P., Landi, E., Mason, H. E., Monsignori Fossi, B. C., & Young, P. R. 1997, A&AS, 125, doi:10.1051/aas:1997368

Doschek, G. A., Warren, H. P., Mariska, J. T., et al. 2008, ApJ, 686, 1362

Fang, X., Yuan, D., Van Doorsselaere, T., Keppens, R., & Xia, C. 2015, ApJ, 813, 33

Fleck, B., & Schmitz, F. 1991, A&A, 250, 235

Gupta, G. R., Banerjee, D., Teriaca, L., Imada, S., & Solanki, S. 2010, ApJ, 718, 11

Hannah, I. G., Hudson, H. S., Battaglia, M., et al. 2011, Space Sci. Rev., 159, 263

Hansteen, V. H., De Pontieu, B., Rouppe van der Voort, L., van Noort, M., & Carlsson, M. 2006, ApJ, 647, L73

Hara, H., Watanabe, T., Harra, L. K., et al. 2008, ApJ, 678, L67

Harten, A., Lax, P. D., & van Leer, B. 1983, SIAM REVIEW, 25, 35

Heggland, L., De Pontieu, B., & Hansteen, V. H. 2007, ApJ, 666, 1277

Jess, D. B., Reznikova, V. E., Van Doorsselaere, T., Keys, P. H., & Mackay, D. H. 2013, ApJ, 779, 168

Jiao, F., Xia, L., Li, B., et al. 2015, ApJ, 809, L17

Keppens, R., Meliani, Z., van Marle, A. J., et al. 2012, Journal of Computational Physics, 231, 718

Kiddie, G., De Moortel, I., Del Zanna, G., McIntosh, S. W., & Whittaker, I. 2012, Sol. Phys., 279, 427

King, D. B., Nakariakov, V. M., Deluca, E. E., Golub, L., & McClements, K. G. 2003, A&A, 404, L1

Klimchuk, J. A. 2015, Philosophical Transactions of the Royal Society of London Series A, 373, 20140256

Koren, B. 1993, A robust upwind discretization method for advection, diffusion and source terms (Centrum voor Wiskunde en Informatica Amsterdam)

Krishna Prasad, S., Banerjee, D., & Gupta, G. R. 2011a, A&A, 528, L4

—. 2011b, A&A, 528, L4

Krishna Prasad, S., Banerjee, D., Van Doorsselaere, T., & Singh, J. 2012, A&A, 546, A50

Landi, E., Young, P. R., Dere, K. P., Del Zanna, G., & Mason, H. E. 2013, ApJ, 763, 86

Maltby, P., Avrett, E. H., Carlsson, M., et al. 1986, ApJ, 306, 284

Marsh, M. S., Walsh, R. W., & Plunkett, S. 2009, ApJ, 697, 1674

McIntosh, S. W., & De Pontieu, B. 2009, ApJ, 707, 524

McIntosh, S. W., Innes, D. E., de Pontieu, B., & Leamon, R. J. 2010, A&A, 510, L2

McIntosh, S. W., & Jefferies, S. M. 2006, ApJ, 647, L77

Nakariakov, V. M., Verwichte, E., Berghmans, D., & Robbrecht, E. 2000, A&A, 362, 1151

Nisticò, G., Nakariakov, V. M., & Verwichte, E. 2013, A&A, 552, A57

Nisticò, G., Pascoe, D. J., & Nakariakov, V. M. 2014, A&A, 569, A12

Nordlund, Å., Stein, R. F., & Asplund, M. 2009, Living Reviews in Solar Physics, 6, doi:10.12942/lrsp-2009-2

Ofman, L., Nakariakov, V. M., & DeForest, C. E. 1999, ApJ, 514, 441

Ofman, L., Wang, T. J., & Davila, J. M. 2012, ApJ, 754, 111

Parker, E. N. 1988, ApJ, 330, 474

Pascoe, D. J., Nakariakov, V. M., & Kupriyanova, E. G. 2013, A&A, 560, A97

Porter, J. G., Toomre, J., & Gebbie, K. B. 1984, ApJ, 283, 879

Porth, O., Xia, C., Hendrix, T., Moschou, S. P., & Keppens, R. 2014, ApJS, 214, 4

Rieutord, M., & Rincon, F. 2010, Living Reviews in Solar Physics, 7, arXiv:1005.5376

Roberts, B. 2006, Philosophical Transactions of the Royal Society of London Series A, 364, 447

Rouppe van der Voort, L., Leenaarts, J., de Pontieu, B., Carlsson, M., & Vissers, G. 2009, ApJ, 705, 272

Samanta, T., Pant, V., & Banerjee, D. 2015, ApJ, 815, L16

Skogsrud, H., Rouppe van der Voort, L., & De Pontieu, B. 2016, ApJ, 817, 124

Snow, B., Botha, G. J. J., & Régnier, S. 2015, A&A, 580, A107

Stein, R. F. 2012, Living Reviews in Solar Physics, 9, doi:10.12942/lrsp-2012-4

Sterling, A. C. 2000, Sol. Phys., 196, 79

Sterling, A. C., Moore, R. L., & DeForest, C. E. 2010, ApJ, 714, L1

Su, J. T., Liu, Y., Liu, S., et al. 2013, ApJ, 762, 42

Su, J. T., Ji, K. F., Banerjee, D., et al. 2016a, ApJ, 816, 30

—. 2016b, ApJ, 816, 30

Su, J. T., Ji, K. F., Cao, W., et al. 2016c, ApJ, 817, 117

Tian, H., McIntosh, S. W., & De Pontieu, B. 2011, ApJ, 727, L37

Tian, H., DeLuca, E., Reeves, K. K., et al. 2014, ApJ, 786, 137

Torrence, C., & Compo, G. P. 1998, Bulletin of the American Meteorological Society, 79, 61

Uritsky, V. M., Davila, J. M., Viall, N. M., & Ofman, L. 2013, ApJ, 778, 26

Verwichte, E., Marsh, M., Foullon, C., et al. 2010, ApJ, 724, L194

Wang, T. 2011, Space Sci. Rev., 158, 397

Wang, T., Ofman, L., & Davila, J. M. 2013, ApJ, 775, L23

Wang, T. J., Ofman, L., & Davila, J. M. 2009a, ApJ, 696, 1448

Wang, T. J., Ofman, L., Davila, J. M., & Mariska, J. T. 2009b, A&A, 503, L25

Yang, L., Zhang, L., He, J., et al. 2015, ApJ, 800, 111

Yuan, D., & Nakariakov, V. M. 2012, A&A, 543, A9

Yuan, D., Nakariakov, V. M., Chorley, N., & Foullon, C. 2011, A&A, 533, A116

Yuan, D., Nakariakov, V. M., Huang, Z., et al. 2014a, ApJ, 792, 41

Yuan, D., Pascoe, D. J., Nakariakov, V. M., Li, B., & Keppens, R. 2015a, ApJ, 799, 221

Yuan, D., Shen, Y., Liu, Y., et al. 2013, A&A, 554, A144

Yuan, D., Sych, R., Reznikova, V. E., & Nakariakov, V. M. 2014b, A&A, 561, A19

Yuan, D., Van Doorsselaere, T., Banerjee, D., & Antolin, P. 2015b, ApJ, 807, 98

Zhang, Y. Z., Shibata, K., Wang, J. X., et al. 2012, ApJ, 750, 16

Zhugzhda, I. D., Locans, V., & Staude, J. 1983, Sol. Phys., 82, 369

Zhugzhda, Y. D. 2008, Sol. Phys., 251, 501

This 2-column preprint was prepared with the AAS LaTeX macros v5.2.

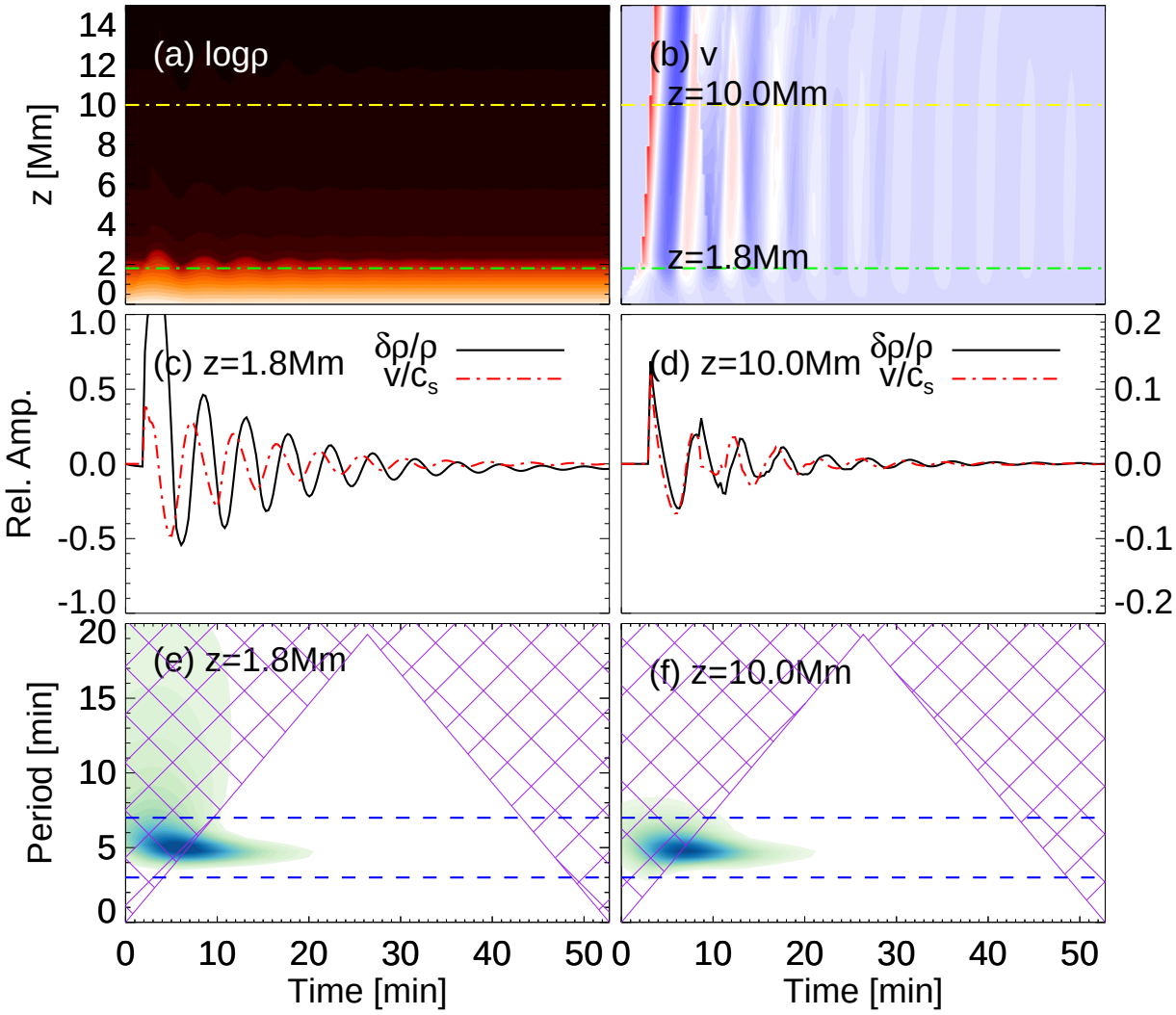

Fig. 4.— (a) and (b) Evolutions of $\log \rho$ and v in the single pulse experiment. Dot-dashed lines mark the positions at 1.8 Mm and 10 Mm where time series are extracted. (c) and (d) Time series of the relative density perturbation $\delta\rho/\rho$ and velocity v/c_s extracted at $z = 1.8$ Mm and $z = 10.0$ Mm, respectively, where c_s is the local sound speed. (e) and (f) Wavelet spectra of the relative density perturbations plotted in (c) and (d), respectively. Blue dashed lines enclose the resonance period range between 3-7 min. The Cone-of-Influence is cross-hatched, within which spectrum should be considered as unreliable.

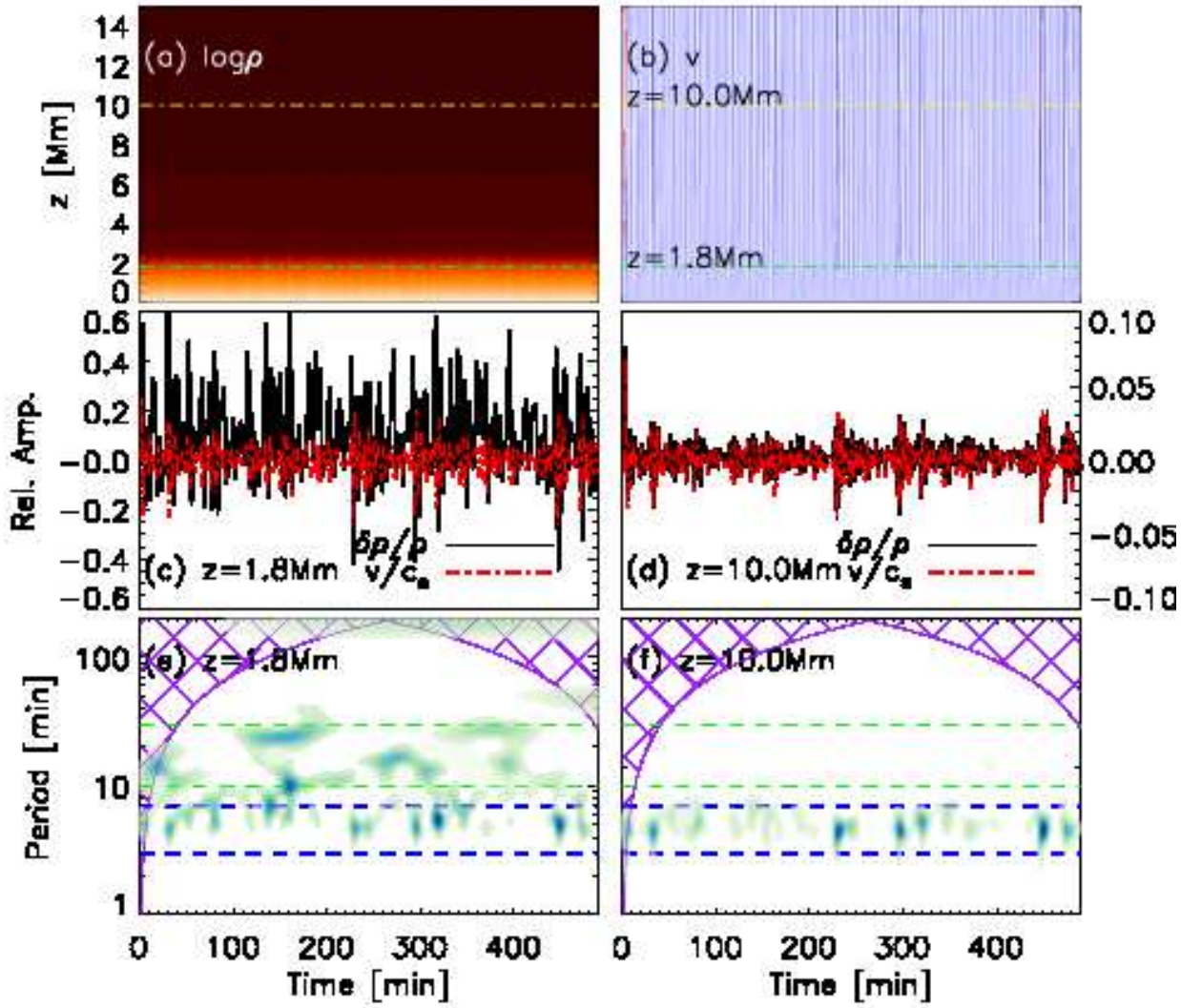

Fig. 5.— Same as Figure 4, but with a stochastic driver. Two green dashed lines labels the quasi-periodic long period oscillations brought in by the stochastic driver as illustrated in Figure 1, whereas two blue dashed lines enclose the resonance period range, as shown in Figure 4. The Cone-of-Influence is cross-hatched, within which spectrum should be considered as unreliable.

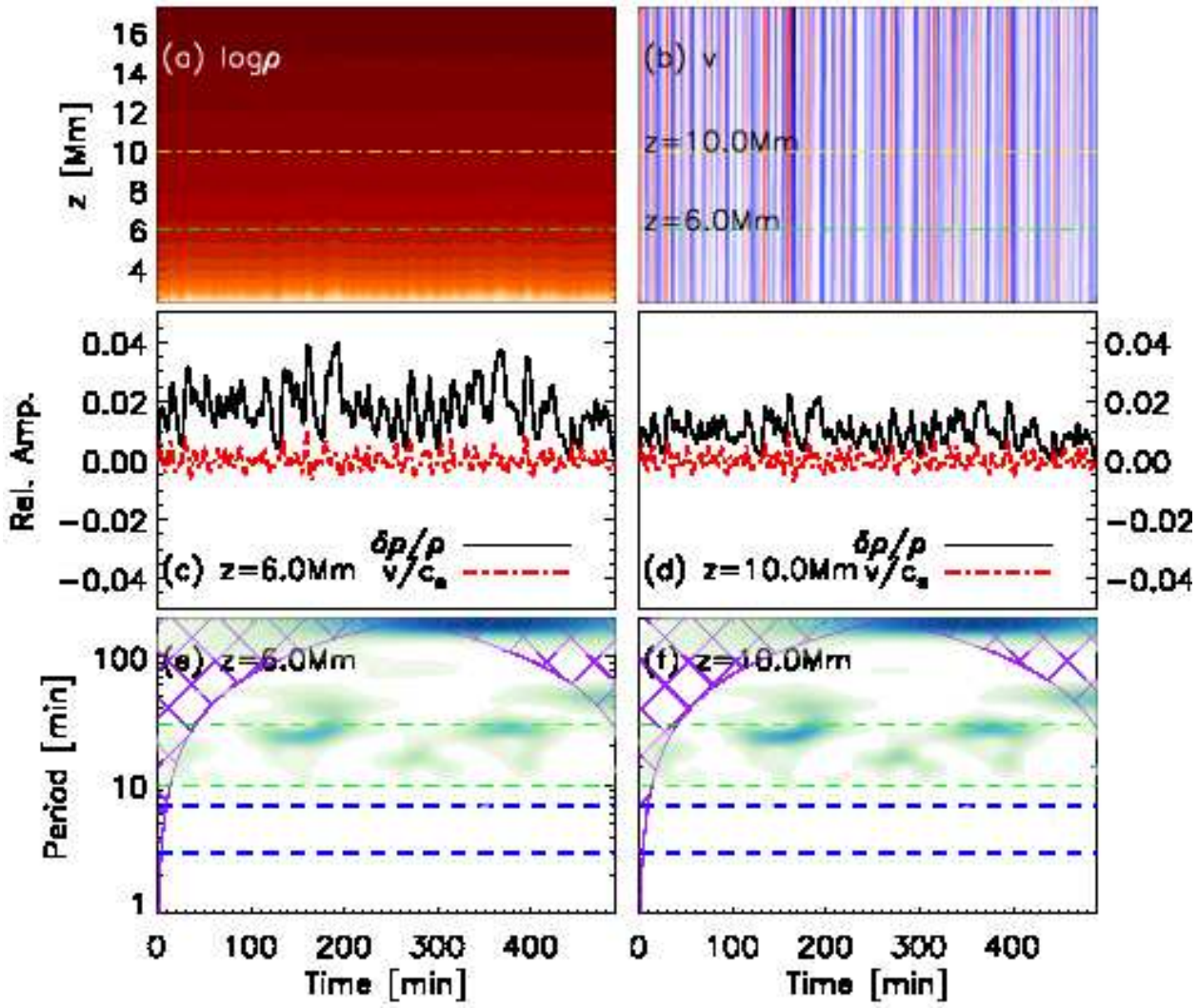

Fig. 6.— Same as Figure 5, but with the driver implemented at $z = 2.3$ Mm and time series were extracted at $z = 6$ Mm and $z = 10$ Mm, respectively. Two green dashed lines labels the quasi-periodic long period oscillations brought in by the stochastic driver as illustrated in Figure 1, whereas two blue dashed lines enclose the resonance period range, as shown in Figure 4. The Cone-of-Influence is cross-hatched, within which spectrum should be considered as unreliable.

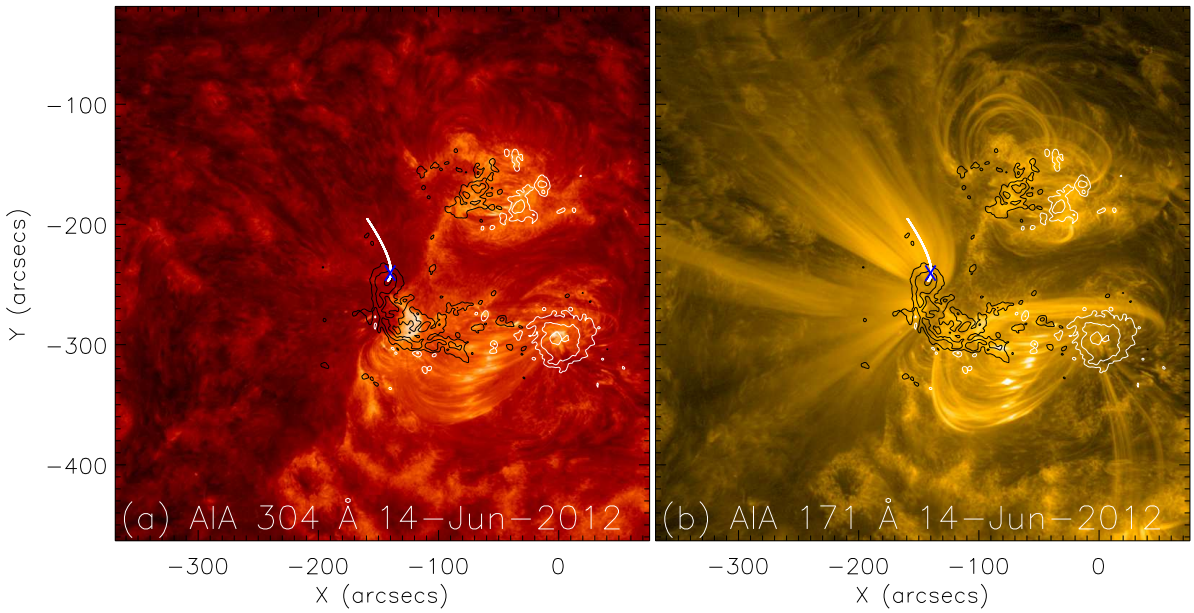

Fig. 7.— Field-of-view (FOV) of AR 11504 observed by the SDO/AIA 304 Å (a) and 171 Å (b) channels on 14 Jun 2012. The Helioseismic and Magnetic Imager (HMI) Line-of-sight magnetogram is contoured at ± 1800 G, ± 900 G, ± 300 G. White and black contours are north and south polarities, respectively. The white slice follows a coronal loop, and the blue cross labels the positions where time series are extracted for wavelet analysis in Figure 8.

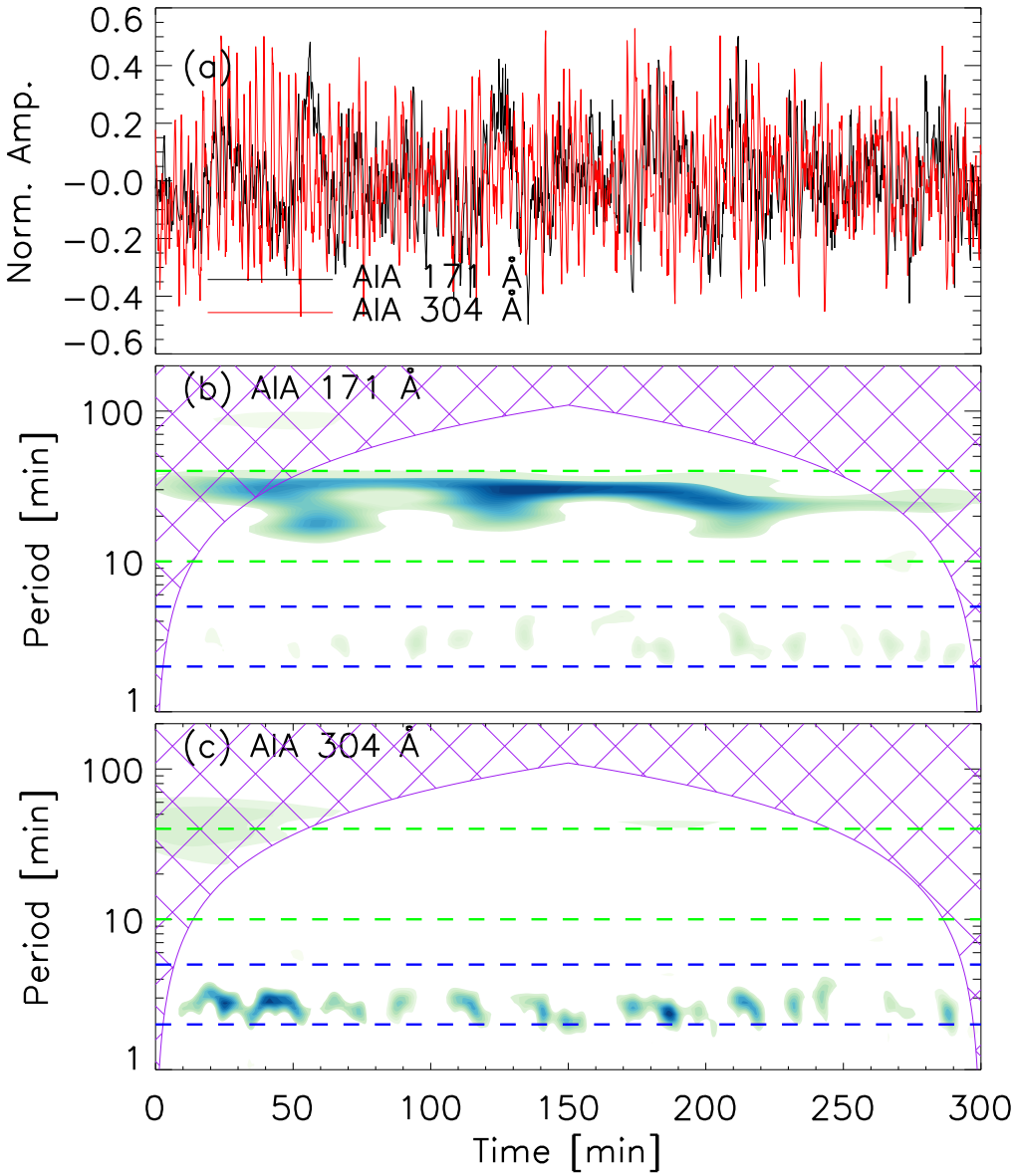

Fig. 8.— (a) Time series of relative emission intensity extracted at a coronal loop marked in Figure 7. The peak-to-peak amplitude is normalized to ±0.5. (b) and (c) are the wavelet spectra for the AIA 171 Å and 304 Å, respectively. The start time is 16:00 UT 14 Jun 2012. Two green dashed lines labels the quasi-periodic long period oscillations at 10-30 min, whereas two blue dashed lines enclose oscillations at 3 min band. The Cone-of-Influence is cross-hatched, within which spectrum should be considered as unreliable.

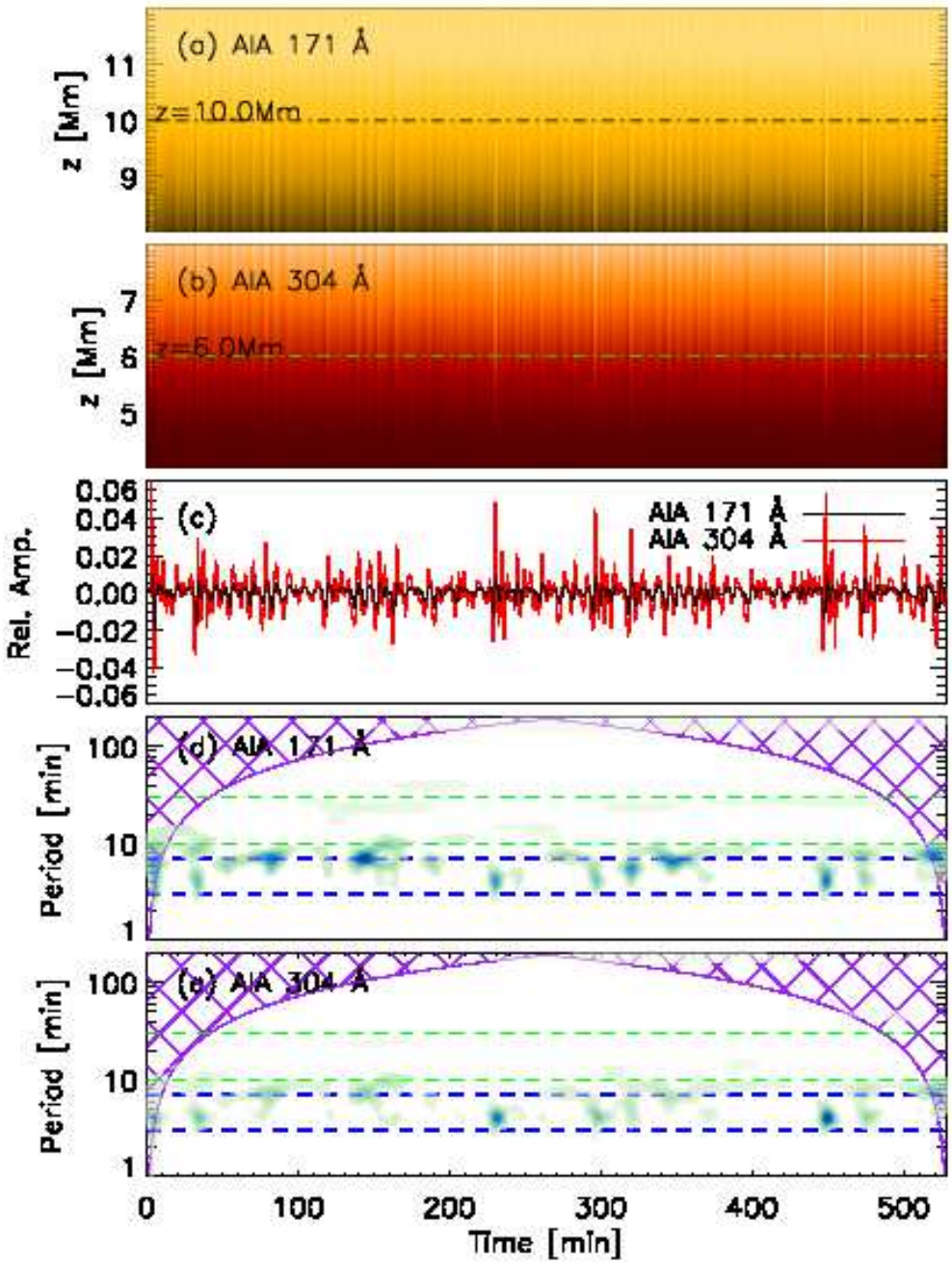

Fig. 9.— (a) and (b) Evolution of the synthetic AIA 171 Å and 304 Å emission intensities for the simulation with driver applied at $z = 0$ Mm. The black dot-dashed line labels the height at $z = 10$ Mm, where a time series is extracted and analysed by wavelet transform; The green dot-dashed line denotes the height at $z = 6$ Mm where the 304 Å counterpart is obtained: time series and wavelet power spectrum. (c) Relative intensity variations of 304 Å extracted at $z = 6$ Mm and 171 Å at $z = 10$ Mm, respectively. (d) and (f) The wavelet power spectrum for the relative intensity variation of 304 Å and 171 Å, respectively. The Cone-of-Influence is cross-hatched, within which spectrum should be considered as unreliable. Two green dashed lines labels the quasi-periodic long period oscillations brought in by the stochastic driver as illustrated in Figure 1, whereas two blue dashed lines enclose the resonance period range, as shown in Figure 4.

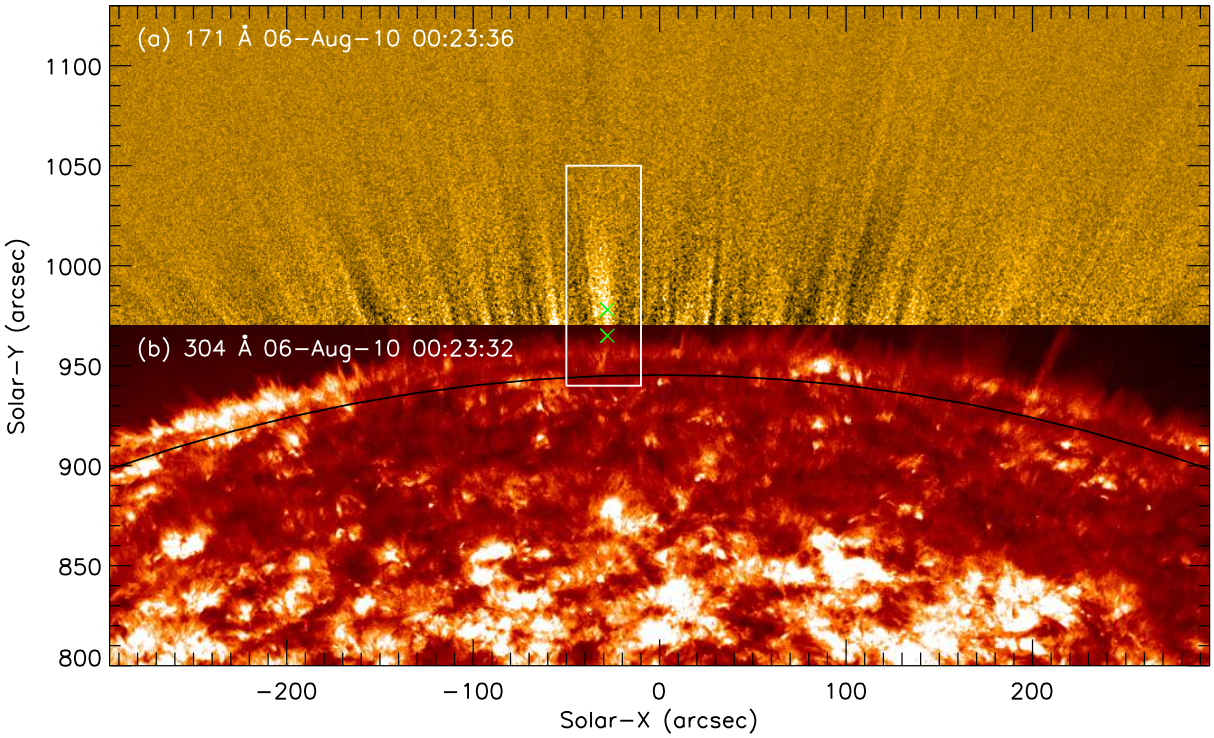

Fig. 10.— A northern coronal hole observed by the AIA 171 Å (a) and 304 Å (b) channels on 06 August 2010. A white rectangle marks the plume of interest: its base is observed by the 304 Å channel, while the upper part is visible in 171 Å. Two time series were extracted at both channels (green crosses) and analysed in Figure 11.

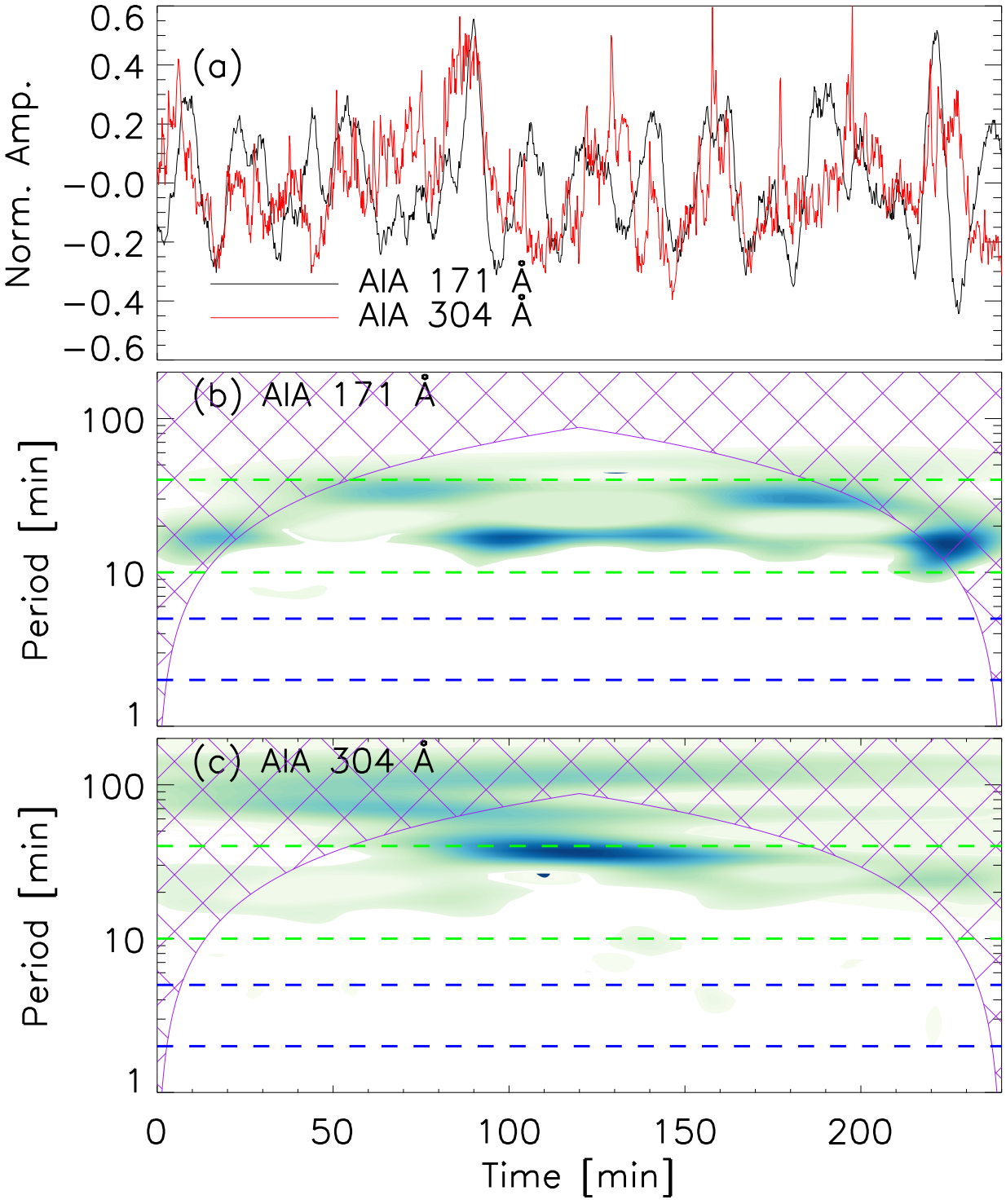

Fig. 11.— Same analysis as in Figure 8, but for the time series extracted at a plume as labeled in Figure 10. Two green dashed lines label the quasi-periodic long period oscillations at 10-30 min, whereas two blue dashed lines enclose oscillations at 3 min band. The Cone-of-Influence is cross-hatched, within which spectrum should be considered as unreliable.

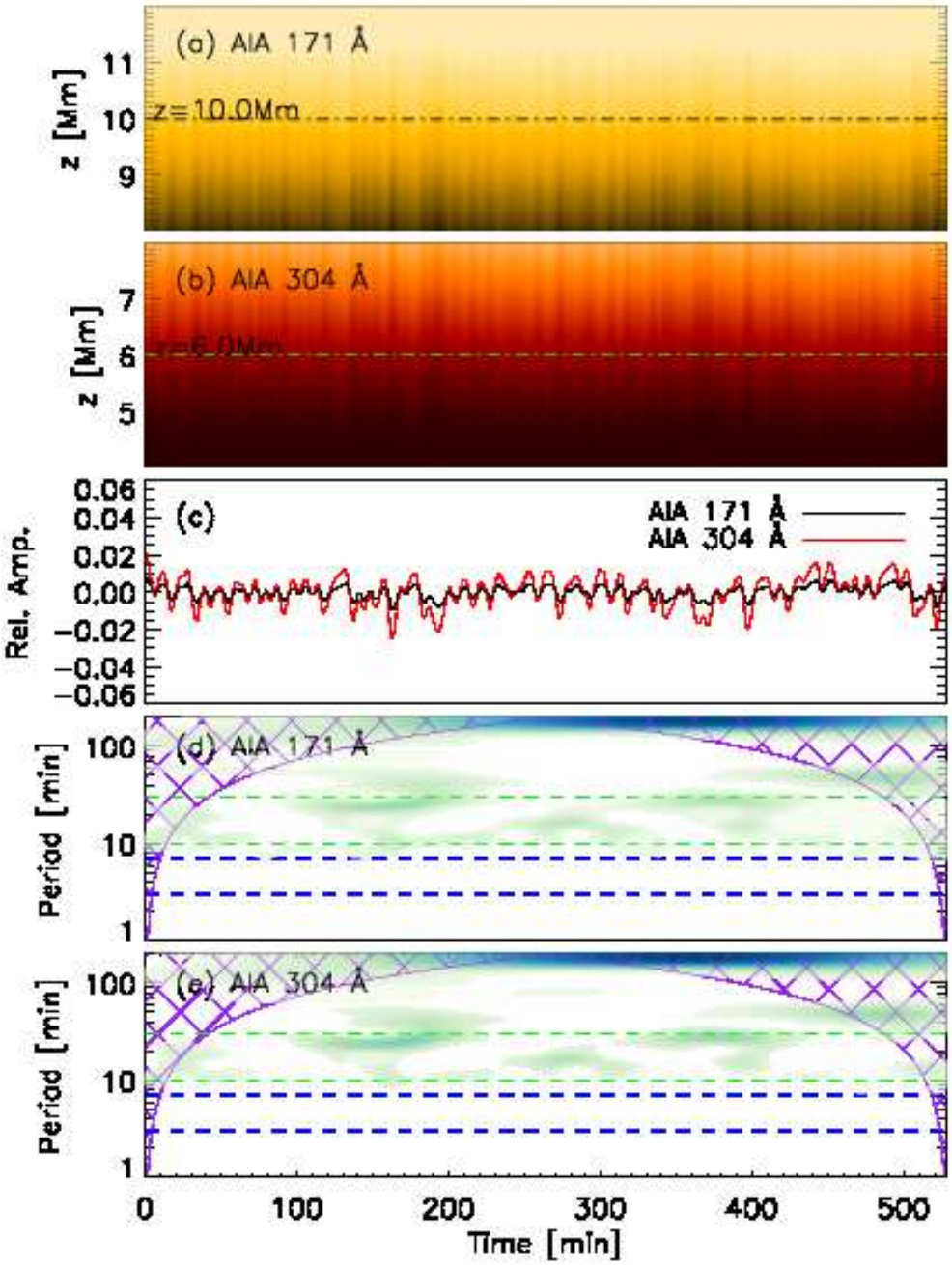

Fig. 12.— Same as Figure 9, but for the simulation with driver applied at $z = 2.3$ Mm. The Cone-of-Influence is cross-hatched, within which spectrum should be considered as unreliable. Two green dashed lines labels the quasi-periodic long period oscillations brought in by the stochastic driver as illustrated in Figure 1, whereas two blue dashed lines enclose the resonance period range, as shown in Figure 4.